Supporting Information

Electrodeposited Cu-Pd Bimetallic Catalysts for the Selective Electroreduction of CO_2 to Ethylene

Ruting Feng,[a] Qinggong Zhu,[b] Mengen Chu,[a] Shuaiqiang Jia,[a] Jianxin Zhai,[a] Haihong Wu,*[a] Peng Wu,*[a] Buxing Han,*[a,b]

[a] Shanghai Key Laboratory of Green Chemistry and Chemical Processes, School of Chemistry and Molecular Engineering, East China Normal University, Shanghai 200062, P. R. China

[b] Beijing National Laboratory for Molecular Sciences, CAS Key Laboratory of Colloid and Interface and Thermodynamics, CAS Research/Education Center for Excellence in Molecular Sciences, Institute of Chemistry, Chinese Academy of Sciences, Zhongguancun North First Street 2, Beijing, 100190, P. R. China

E-mail: hhwu@chem.ecnu.edu.cn; pwu@chem.ecnu.edu.cn; hanbx@iccas.ac.cn

Contents

Experimental Section

Materials

Palladium (II) sulfate ($PdSO_4$), Copper (II) sulfate ($CuSO_4 \cdot 5H_2O$), sulfuric acid (H_2SO_4), Toray Carbon Paper (CP, TGP-H-60, 19 cm × 19 cm), and Nafion N-117 membrane (0.180 mm thick, ≥ 0.90 meg/g exchange capacity) were purchased from Alfa Aesar China Co., Ltd. Both CO_2 and N_2 had a purity of 99.999%, and were provided by Shanghai Chemistry Industrial Zone Pujiang Special Type Gas Co., Ltd.

Preparation of Cu-Pd bimetallic catalysts

Electrochemical deposition was carried out using a solution of 0.1 M $CuSO_4$, 1 mM $PdSO_4$, and 0.1 M H_2SO_4 in a 50 mL electrolytic tank. Carbon paper and Pt gauze with 1 cm^2 area each acted as cathode and anode. The electrodeposition was conducted by high resolution DC power supply (HY3005B, Hangzhou Huayi Electronics Industry Co., Ltd.) which outputted a steady current for desired time.

Other electrocatalysts (Cu-Pd/CP-CV, Cu-Pd/CP-IT) were synthesized by electrochemical workstation (Voltammetry and Amperometric-i-t) in three electrode system for comparison. The number of electrons was controlled to 12 coulombs, cyclic voltammetry and Amperometry were performed at -0.2 V with scan rate 50 mv s^{-1}, respectively.

Characterization

The morphology of the electrodes was characterized by Hitachi S4800 scanning electron microscope (SEM) at 3 kV and transmission electron microscopy (TEM, JEOL JEM-2100F) equipped with EDS. X-ray diffraction (XRD) analysis of the samples were performed on Rigaku and model with CuKα radiation (1.5418 Å). X-ray photoelectron spectroscopy (XPS) study was carried out on the AXIS Supra surface analysis instrument with an X-ray monochromatic source (combined Al/Ag anode, energy 1486.6/2984.2eV) and studies were performed in 10^{-9} mbar vacuum.

Electrochemical study

All the electrochemical experiments were conducted on the electrochemical workstation (CHI 660E, Shanghai CH Instruments Co., China). Linear sweep voltammetry (LSV) measurement was carried out in a two-compartment H-cell separated by an ion exchange membrane (Nafion 117) with three electrodes on an electrochemical workstation (CHI 660E, Shanghai CH Instruments Co., China), which were a working electrode (Cu-Pd), a platinum gauze auxiliary electrode, and an Ag/AgCl (3M KCl). 0.1 M KCl solution and 0.1 M $KHCO_3$ solution were utilized as the cathode and anodic electrolytes, respectively.[1] In all measurements, we used Ag/AgCl as the reference electrode, and the potential (vs. Ag/AgCl) was converted to RHE using the following equation[2]:

$$E(RHE) = E(Ag/AgCl) + 0.197 + 0.059 \times pH$$

The electrolytes were bubbled with CO_2 or N_2 at least 30 min to ensure formation of N_2-saturated or CO_2-saturated solution before experiments. LSV measurements in gas-saturated electrolytes were carried out in the potential range of 0 V to -1.4 V versus RHE at a sweep rate of 50 mV s^{-1}. Slight magnetic stirring was employed to acquire uniform electrolytes.

Electrochemical impedance spectroscopy (EIS) measurements

The experimental apparatus was the same as that used for the LSV measures. Measurements were carried out in CO_2-saturated 0.1 M KCl solution at an open circuit potential (OCP) with a frequency range from 10^{-2} Hz to 10^5 Hz and the amplitude was 5 mV. The data were fitted by View® software (Version 2.9c, Scribner Associates, USA).

CO_2 reduction electrolysis

The electroreduction of CO_2 was performed at room temperature in a gas-tight H-type electrolysis cell separated by an ion exchange membrane (Nafion 117), which is equipped with a three-electrode system including a working electrode (Cu-Pd), a platinum gauze auxiliary electrode, and an Ag/AgCl (3 M KCl) reference electrode. In the experiments, 0.1 M KCl (30 mL) solution and 0.1 M $KHCO_3$ (30 mL) solution were utilized as catholyte and anolyte, respectively. Before the electrolysis, CO_2 was bubbled through the cathodic electrolyte for 30 min to remove the air and form a CO_2-suturated solution. The reaction was performed with a steady flow of CO_2 (10 sccm) at a constant potential. Before electrolysis, the cathode was electrochemically reduced using cyclic voltammetry (CV), which ranged from 0 to -1.4V (vs. RHE) at a scan rate of 100 mV s^{-1} for 5 cycles to remove the possible oxidized species.

Product analysis

After the electrolysis reaction, the gas-phase products were analyzed by a gas chromatograph (GC; Agilent-8890A)，which was equipped with TCD detector. The liquid product was quantified using a nuclear magnetic resonance (NMR) spectrometry (Bruker, Ascend 400-400 MHz) in [D_6] DMSO with phenol as the internal standard. The Faradaic efficiency (FE) of the products was calculated using $FE=\alpha nF/Q$, where α is the number of electrons transferred in the electrochemical reaction, n is the number of moles for a given products, F is Faraday's constant (96485 C mol^{-1}), and Q represents all the charge passed throughout the electrolysis process.

Double-layer capacitance (C_{dl}) measurements.

The electrochemical active surface area is proportional to C_{dl} value. C_{dl} was determined in H-type electrolysis cell by measuring the capacitive current associated

with double-layer charging from the scan-rate dependence of cyclic voltammogram (CV). The CV ranged from -1.35 V -1.45 V vs. Ag/AgCl. The C_{dl} was estimated by plotting the Δj (j_a-j_c) at -1.35 V vs Ag/AgCl against the scan rates, in which the j_a and j_c were the anodic and cathodic current density, respectively.

Supplementary Figures

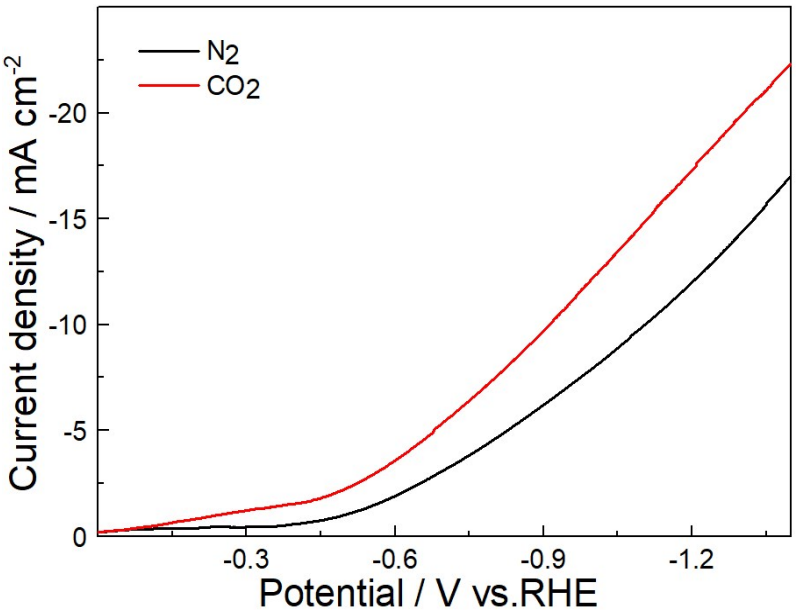

Figure S1. LSV of Cu-Pd/CP in N_2-and CO_2-saturated 0.1 M KCl.

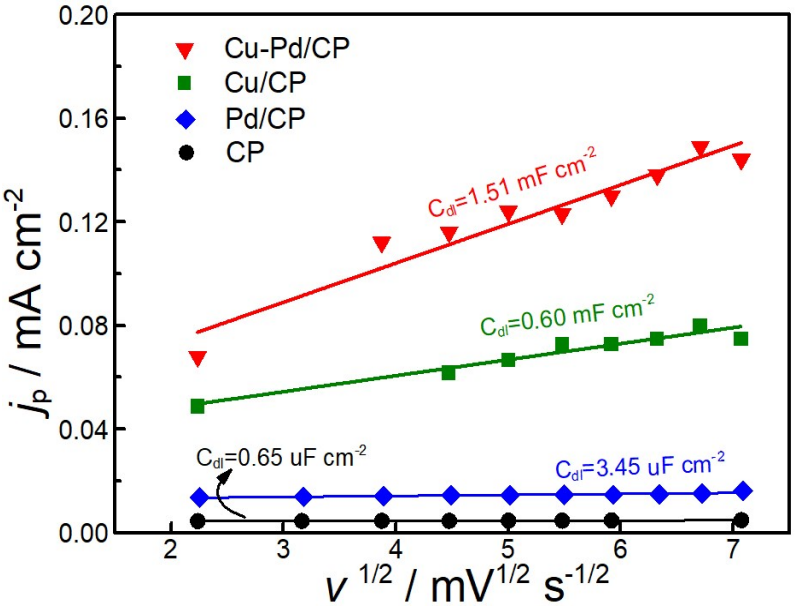

Figure S2. Charging current density against scan rates over different electrodes in CO_2 saturated 0.1 M KCl electrolyte.

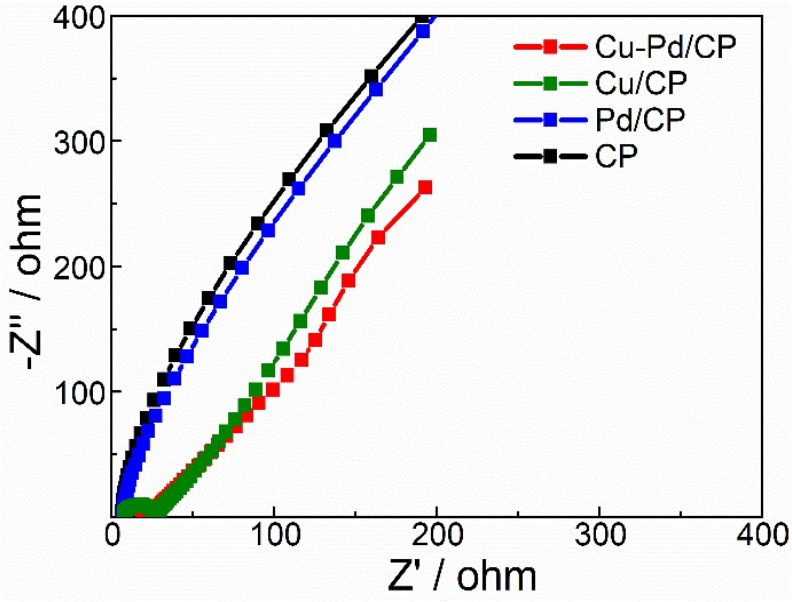

Figure S3. Nyquist plots over the four electrodes (CP, Cu/CP, Pd/CP and Cu-Pd/CP).

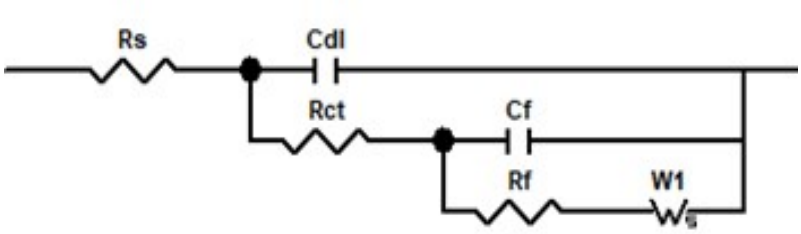

Figure S4. Equivalent circuit used for fitting the data of Nyquist plots. The components contain solution resistance (Rs), double layer capacitance (CPE_{dl}), electron transfer resistance (R_{ct}), film capacitance (C_f), film resistance (Rf) and Warburg-type impedance (Z_w).

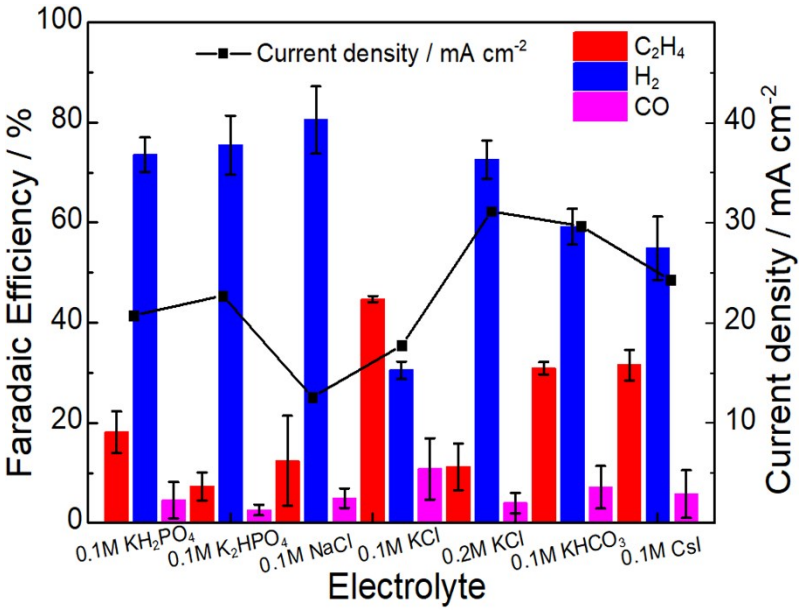

Figure S5. The FE of C_2H_4 over Cu-Pd/CP catalyst in various electrolytes at -1.2 V vs. RHE.

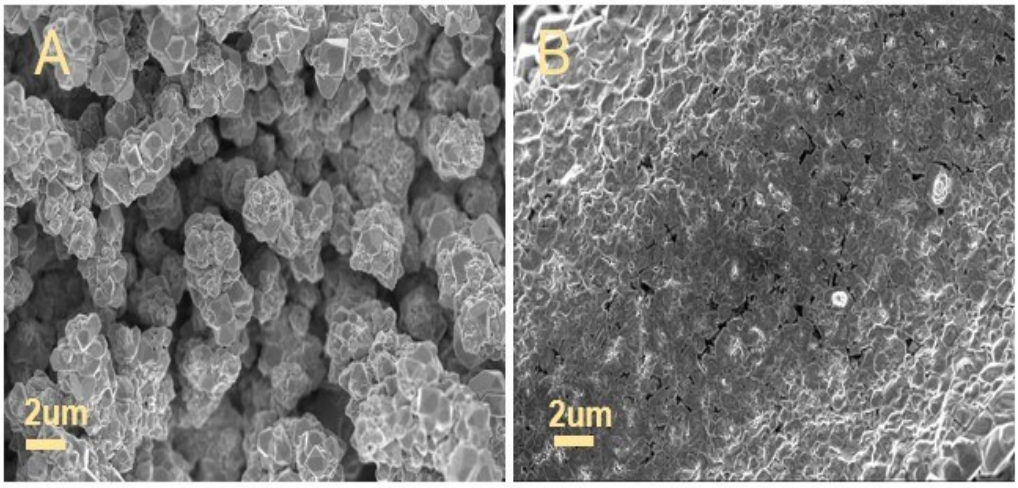

Figure S6. SEM images: A) Cu-Pd/CP-CV catalyst; B) Cu-Pd/CP-IT catalyst.

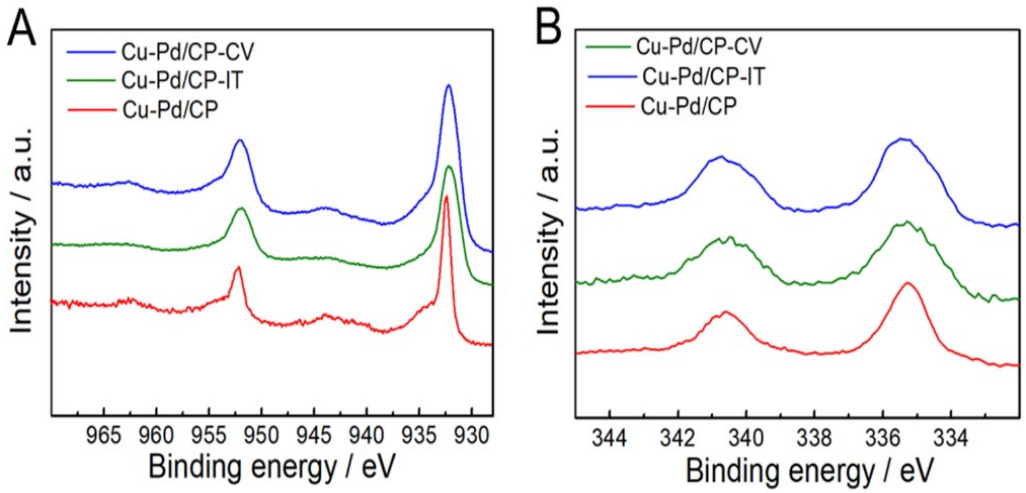

Figure S7. XPS spectra of: A) Cu 2p, B) Pd 3d XPS spectra of Cu-Pd/CP, Cu–Pd/CP-CV and Cu-Pd/CP-IT.

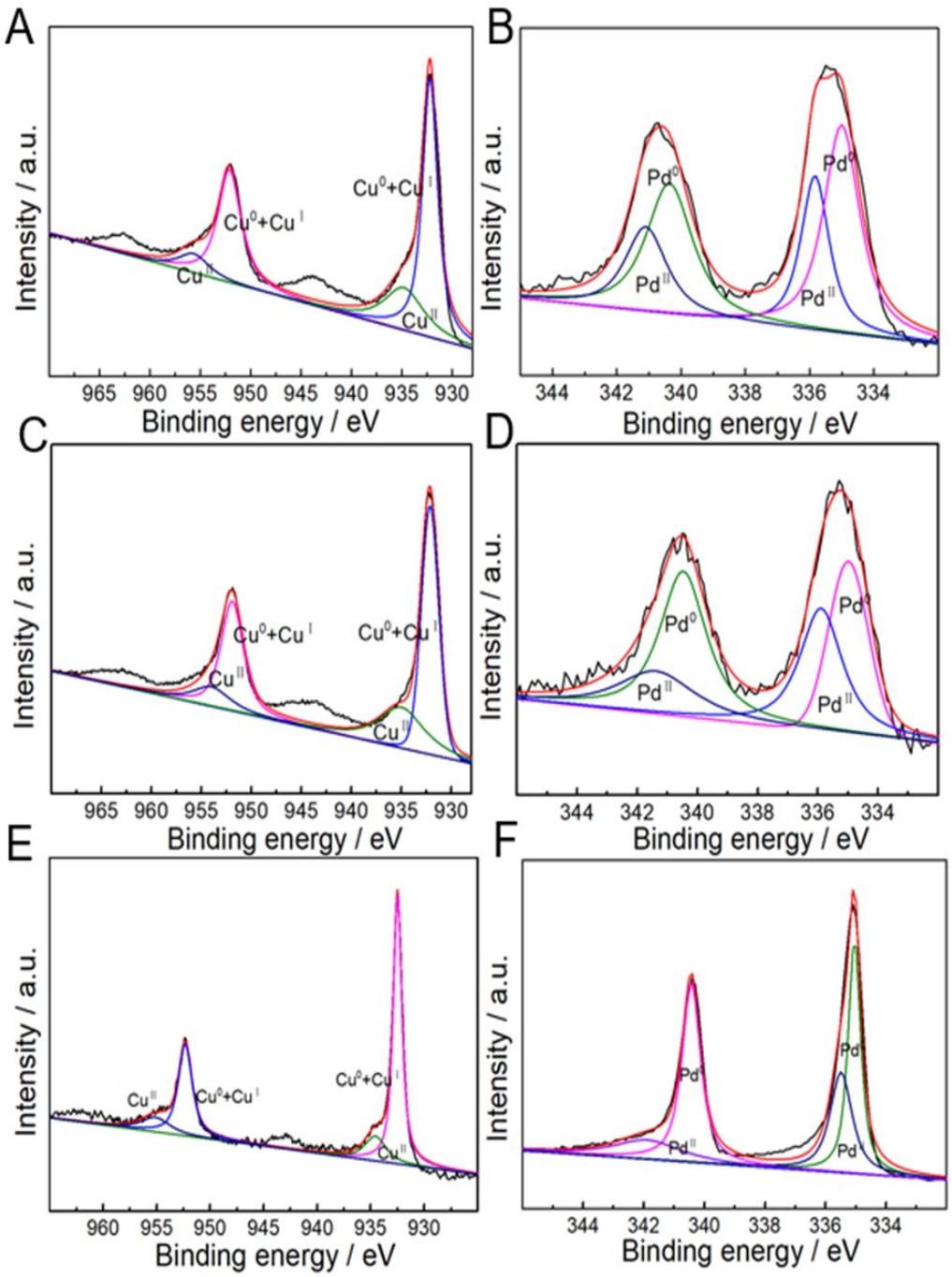

Figure S8. XPS spectras of Cu 2p of A) Cu-Pd/CP-CV and C) Cu-Pd/CP-IT catalysts, Pd3p of B) Cu-Pd/CP-CV and D) Cu-Pd/CP-IT. E) Cu/CP and F) Pd/CP.

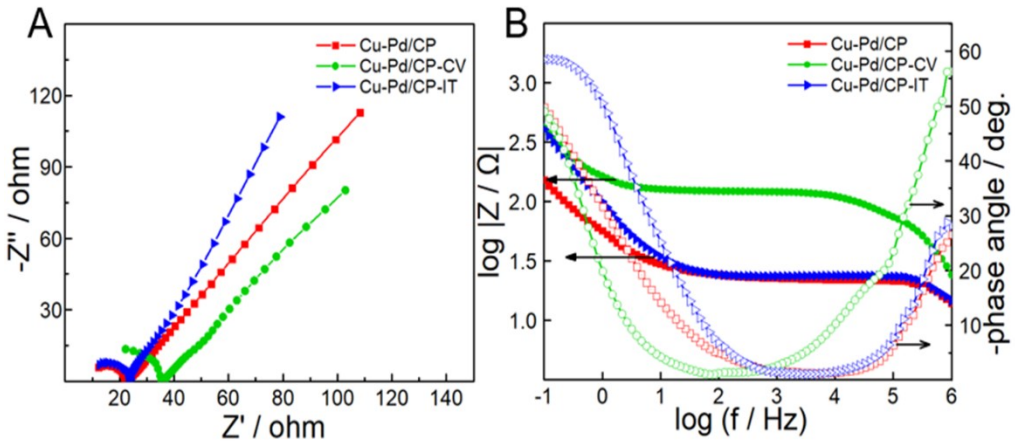

Figure S9. A) Nyquist plots B) and C) Bode plots obtained for three electrodes (Cu-Pd/CP, Cu-Pd/CP-CV, Cu-Pd/CP-IT) in CO_2-saturated 0.1 M KCl solution.

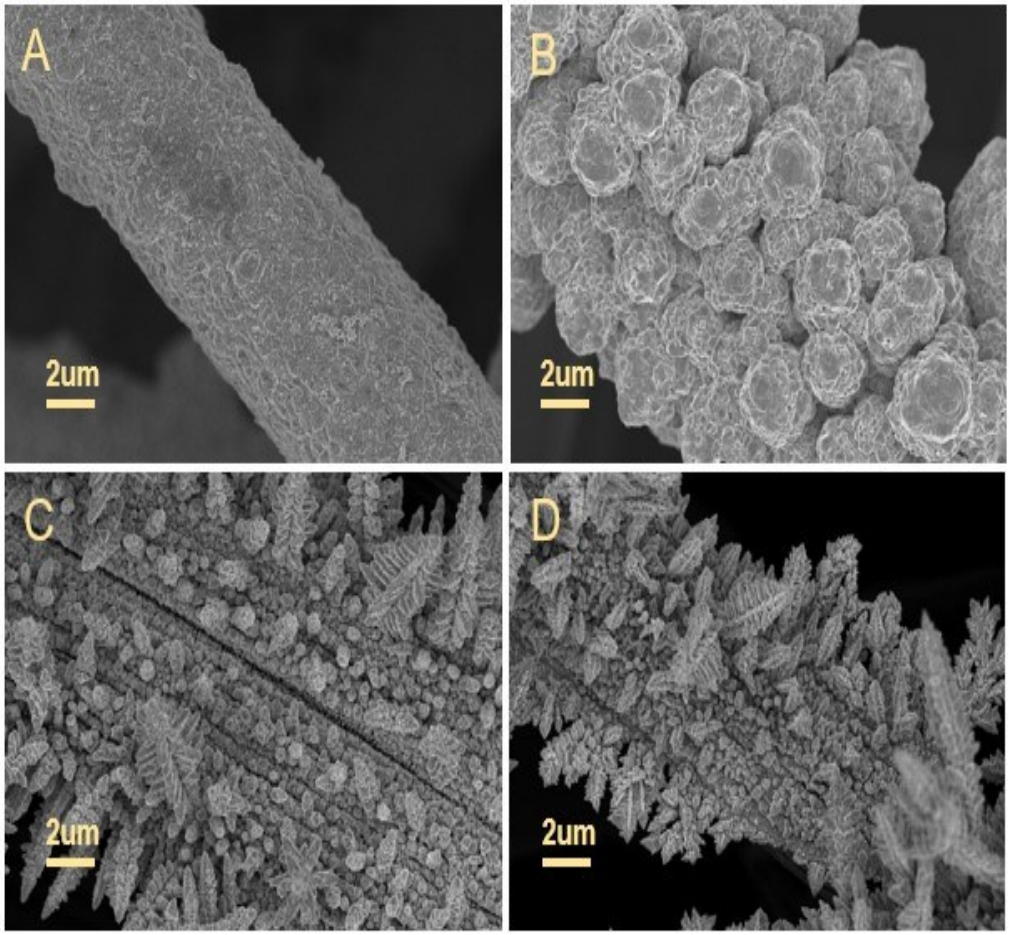

Figure S10. SEM images of Cu-Pd/CP catalysts under the deposition current of A) 8.7mA (-0.1 V), B) 25.4 mA (-0.4 V), C) 26 mA (-0.6 V), D) 32.5 mA (-0.8 V) vs. Ag/AgCl.

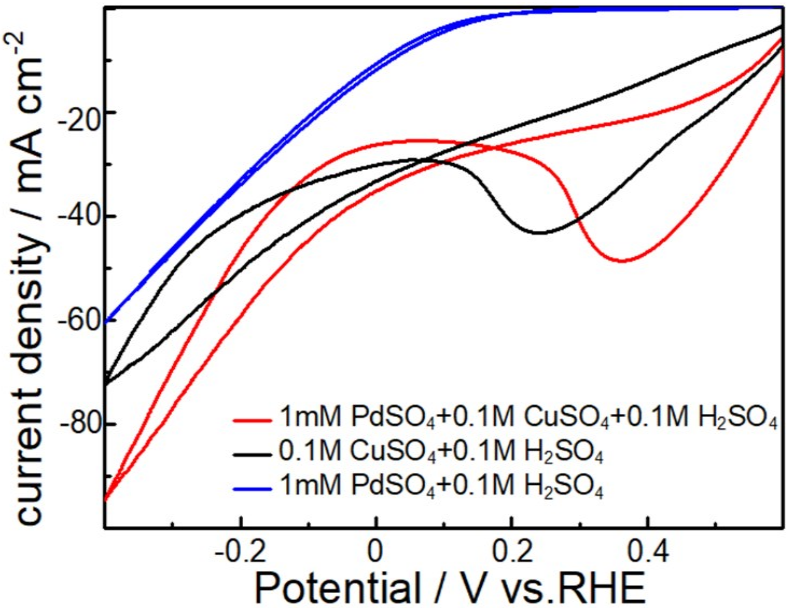

Figure S11. Cyclic voltammetry curves of bulk carbon paper in three electroplating baths.

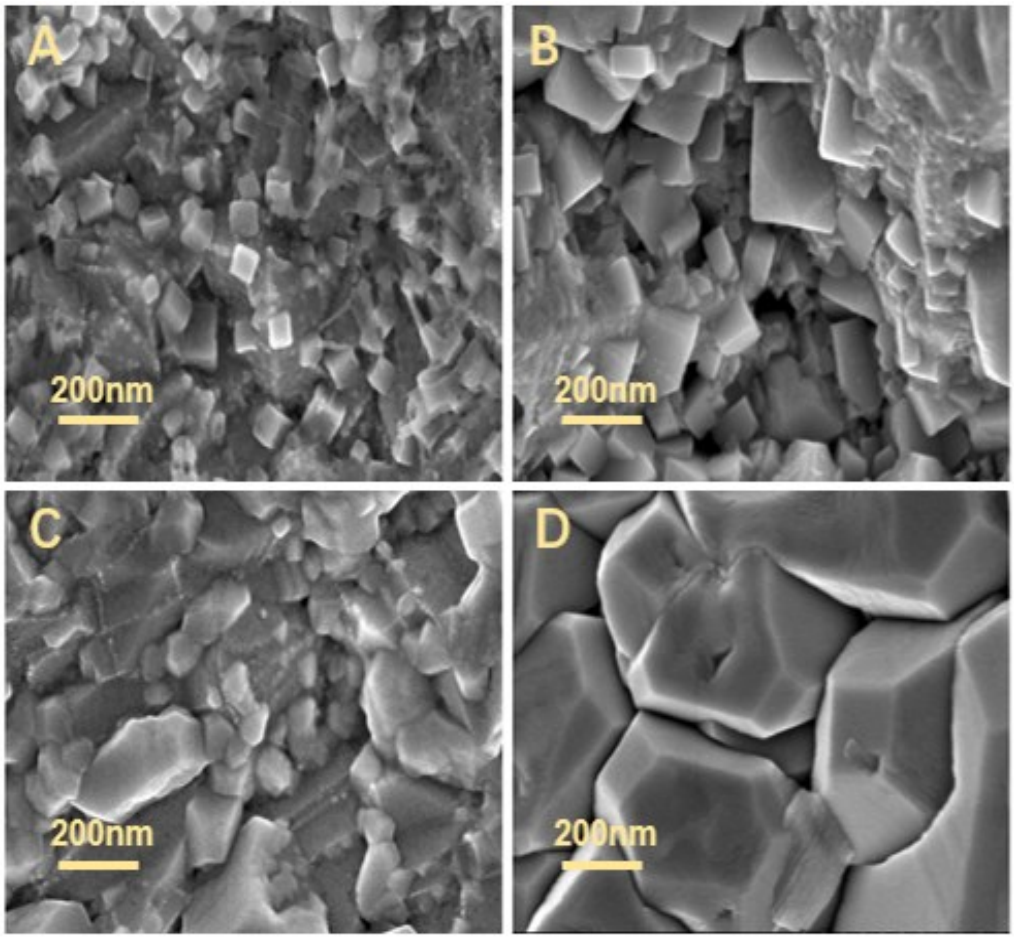

Figure S12. SEM images of A) 5 min, B) 10 min, C) 15 min, D) 20 min deposition time at 20 mA cm^{-2}.

Supplementary Tables

Table S1. Comparison of the results of CO_2 electroreduction to ethylene over various Cu-based composite electrocatalysts.

Electrocatalyst	Potential / V	Electrolyte	FE/%	Current density / mA cm^{-2}	Ref.
H-type cell					
Bimetallic Cu-Pd catalysts	-1.2 V vs. RHE	0.1 M KCl	45.2	17.4	This work
Cu_{10}-Sb_1	-1.19 V vs. RHE	0.1 M KCl	49.5	28.5	[2]
Ag/Cu nanocrystals	–1.1 V vs. RHE	0.1 M $KHCO_3$	40	1.0	[3]
Carbon–supported Cu catalyst	–2.2 V vs. Ag/AgCl	0.1 M $KHCO_3$	45	22.5	[4]
Ag-Cu arrays	-1.2 V vs. RHE	0.5 M $KHCO_3$	41.3	8.45	[5]
Cu_2O/rGO	-1.4 V vs. RHE	0.1 M $KHCO_3$	19.7	12	[6]
Cu-C_3N_4	1.6 V vs Ag/AgCl	0.1 M $KHCO_3$	10	~7.5	[7]
Cu-Zn bimetallic catalyst	–1.1 V vs. RHE	0.1 M $KHCO_3$	33.3	6.1	[8]
Cu/$ICTF_{50}$	-1.3 V vs. RHE	0.1 M KCl+ 0.1 M $KHCO_3$	34	11.8	[9]
4H Au@Cu nanoribbon	-1.11 V vs RHE	0.1 M $KHCO_3$	44.9	30.2	[10]
GMC-[Cu_2(NTB)$_2$]	-1.27 V vs RHE	0.1 M KCl	40	13	[11]
Flow cell					
Cu/N-CNF	-0.57 V vs. RHE	5 M KOH	62	600	[12]
Cu@Cu_xO	-1.58 V vs. RHE	0.1 M $KHCO_3$	45.8	150	[13]
Electrodeposited CuAg alloy	-0.7 V vs. RHE	1M KOH	60	300	[14]

Table S2. Ratio of Cu/Pd, $(Cu^0+Cu^{I})/Cu^{II}$ and Pd^{II}/Pd^0 calculated from Cu2p and Pd3p signals of three electrodes.

Electrodes	Cu/Pd ratio (by XPS)	Atomic ratio of $(Cu^0+Cu^{I})/Cu^{II}$	Atomic ratio of Pd^0/Pd^{II}
Cu-Pd/CP	6.83	2.48	0.405
Cu-Pd/CP-CV	32.20	3.20	0.625
Cu-Pd/CP-IT	61.20	3.00	0.617

Table S3. Parameter values of the equivalent circuit model.

Electrodes	R_s (Ωcm^{-2})	R_{ct} (Ω cm^{-2})	R_f (Ω cm^{-2})
Cu-Pd/CP	8.756	13.35	2.50
Cu-Pd/CP-CV	9.449	15.42	10.50
Cu-Pd/CP-IT	10.540	15.90	2.51

References

[1] X. Sun, Q. Zhu, X. Kang, H. Liu, Q. Qian, Z. Zhang, B. Han, *Angew. Chem. Int. Ed.* **2016**, *55*, 6771-6775.

[2] S. Jia, Q. Zhu, H. Wu, M. e. Chu, S. Han, R. Feng, J. Tu, J. Zhai, B. Han, *Chinese. J. Catal.* **2020**, *41*, 1091-1098.

[3] J. Huang, M. Mensi, E. Oveisi, V. Mantella, R. Buonsanti, *J. Am. Chem. Soc.* **2019**, *141*, 2490-2499.

[4] O. A. Baturina, Q. Lu, M. A. Padilla, L. Xin, W. Li, A. Serov, K. Artyushkova, P. Atanassov, F. Xu, A. Epshteyn, T. Brintlinger, M. Schuette, G. E. Collins, *Acs. Catal.* **2014**, *4*, 3682-3695.

[5] L. Hou, J. Han, C. Wang, Y. Zhang, Y. Wang, Z. Bai, Y. Gu, Y. Gao, X. Yan, *Inorganic Chemistry Frontiers* **2020**, *7*, 2097-2106.

[6] H. Ning, Q. Mao, W. Wang, Z. Yang, X. Wang, Q. Zhao, Y. Song, M. Wu, *J. Alloys Compd.* **2019**, *785*, 7-12.

[7] Y. Jiao, Y. Zheng, P. Chen, M. Jaroniec, S. Z. Qiao, *J. Am. Chem. Soc.* **2017**, *139*, 18093-18100.

[8] Y. Feng, Z. Li, H. Liu, C. Dong, J. Wang, S. A. Kulinich, X. Du, *Langmuir* **2018**, *34*, 13544-13549.

[9] M. J. Mao, M. D. Zhang, D. L. Meng, J. X. Chen, C. He, Y. B. Huang, R. Cao, *ChemCatChem* **2020**, *12*, 3530-3536.

[10] Y. Chen, Z. Fan, J. Wang, C. Ling, W. Niu, Z. Huang, G. Liu, B. Chen, Z. Lai, X. Liu, B. Li, Y. Zong, L. Gu, J. Wang, X. Wang, H. Zhang, *J. Am. Chem. Soc.* **2020**.

[11] M. Balamurugan, H. Y. Jeong, V. S. K. Choutipalli, J. S. Hong, H. Seo, N. Saravanan, J. H. Jang, K. G. Lee, Y. H. Lee, S. W. Im, V. Subramanian, S. H. Kim, K. T. Nam, *Small* **2020**, *16*, e2000955.

[12] J.-C. Lee, J.-Y. Kim, W.-H. Joo, D. Hong, S.-H. Oh, B. Kim, G.-D. Lee, M. Kim, J. Oh, Y.-C. Joo, *J. Mater. Chem. A.* **2020**, *8*, 11632-11641.

[13] K. Yao, Y. Xia, J. Li, N. Wang, J. Han, C. Gao, M. Han, G. Shen, Y. Liu, A. Seifitokaldani, X. Sun, H. Liang, *J. Mater. Chem. A.* **2020**, *8*, 11117-11123.

[14] T. T. H. Hoang, S. Verma, S. Ma, T. T. Fister, J. Timoshenko, A. I. Frenkel, P. J. A. Kenis, A. A. Gewirth, *J. Am. Chem. Soc.* **2018**, *140*, 5791-5797.